Boundary condition development for an adverse pressure gradient turbulent boundary layer at the verge of separation

V. Kitsios*[,1], C. Atkinson[1], J. A. Sillero[2], G. Borrell[2], A. G. Gungor[3], J. Jiménez[2] and J. Soria[1,4]

[1] *Laboratory For Turbulence Research in Aerospace and Combustion, Department of Mechanical and Aerospace Engineering, Monash University, Clayton 3800, AUSTRALIA*
[2] *School of Aeronautics, Universidad Politécnica de Madrid, E-28040 Madrid, SPAIN*
[3] *ITU Faculty of Aeronautics and Astronautics, Department of Astronautical Engineering, Maslak 34469 Istanbul, TURKEY*
[4] *Department of Aeronautical Engineering, King Abdulaziz University, Jeddah 21589, KINGDOM OF SAUDI ARABIA*
**E-mail: vassili.kitsios@monash.edu*

Details are provided on the development of a farfield boundary condition for the direct numerical simulation of an adverse pressure gradient (APG) turbulent boundary layer (TBL) at the verge of separation. The APG TBL achieves a region constant pressure velocity to freestream velocity ratio over a momentum thickness based Reynolds number range of $Re_\theta \approx 2000$ to 6000. Mean velocity deficit and Reynolds stress profiles are presented under both friction velocity and pressure velocity based scaling within this range. The pressure velocity scaling demonstrates a collapse of the statistical profiles.

Keywords: Adverse Pressure Gradient; Turbulent Boundary Layer; Direct Numerical Simulation.

1. Introduction

The performance of many engineering systems relies on fluid flows remaining attached to aerodynamic surfaces, and the occurrence of flow separation can potentially result in catastrophic consequences or at best energy efficiency degradation. The study of fluid flow separation is, therefore, of utmost importance. Real world examples include the flow over aerofoil geometries including aircraft wings, wind turbine blades, and turbo-machinery. The accurate prediction of turbulent boundary layer (TBL) separation remains a significant challenge for engineering design. One of the complexities of these aerofoil geometries, however, is that the pressure gradient is constantly changing in the streamwise direction, as in the large eddy simulation of Kitsios et. al. (2011)[1].

In the present study we focus our efforts on the canonical flow configuration of a self-similar TBL subjected to an adverse pressure gradient (APG) such that the TBL is at the verge of separation, akin to the configuration in the experimental study of Skate & Krogstad (1994)[2]. A self-similar APG TBL is defined as having a constant ratio of friction velocity (u_τ) to freestream velocity (u_∞), and also a constant ratio of pressure velocity (u_P) to u_∞ [3]. Previous TBL APG direct numerical simulations (DNS) include the non-self-similar separated flow of Gungor et. al. (2012) [4], and self-similar APG cases at relatively low Reynolds numbers in Lee & Sung (2008) [5]. In the present study we undertake simulations of the incipient separation case on a flat surface using the TBL DNS code of Simens et. al. (2009) [6] and Borrell et. al. (2013) [7], with a modified farfield APG boundary condition (BC). This effectively decouples the effect of upstream flow history and surface curvature from the influence of the local pressure gradient. The maximum momentum number based Reynolds number in present simulations is $Re_\theta = 6000$.

An overview of the original ZPG TBL DNS code is presented in section 2, with the modifications to the BC required to generated the self-similar APG TBL presented in section 3. In section 4, profiles of first and second order statistical moments from the DNS of the APG and ZPG TBLs are presented scaled on the basis of the friction and pressure velocities. Finally concluding remarks are made in section 5.

2. Direct numerical simulation details

The TBL DNS code adopted within solves the Navier-Stokes equations in a three-dimensional rectangular volume, with constant density (ρ) and kinematic viscosity (ν). The three flow directions are the streamwise (x), wall-normal (y) and spanwise (z), with respective instantaneous velocity components in these directions of u, v and w. Note throughout this paper the time averaged velocity components are denoted by ($\overline{u}, \overline{v}, \overline{w}$), where the overline is the time averaging operation, with associated fluctuating components of (u', v', w'). A fractional-step method [8,9] is used to solve the governing equations for the velocity and pressure (p) fields. Fourier decomposition is used in the periodic spanwise direction, with compact finite difference [10] in the aperiodic wall-normal and streamwise directions. The equations are stepped forward in time using a modified three sub-step Runge-Kutta scheme [6].

The code utilises MPI and openMP parallelisation. For each MPI process the physical domain is decomposed into streamwise regions containing all spanwise and wall-normal points. The physical subdomain is further decomposed into wall normal planes for each openMP thread [7]. All spatial derivatives in the spanwise and wall-normal direction can then be calculated with no MPI message passing. To calculate the streamwise derivatives the data is rearranged into streamwise oriented lines [7].

The boundary conditions of the original ZPG version of the TBL DNS code are as follows. The bottom surface is a flat plate with a no-slip (zero velocity) BC. The spanwise boundaries are periodic. Due to the TBL growing in height as it develops in the streamwise direction, a downstream streamwise normal plane is copied, and mapped to the inlet BC [11]. At the farfield boundary the spanwise vorticity is zero, and the wall normal suction velocity is given by

$$v_{ZPG}(x) = \frac{d\delta^*(x)}{dx}\, u_{ZPG}\ , \tag{1}$$

where u_{ZPG} is the constant freestream streamwise velocity, and δ^* is the displacement thickness[12].

3. Adverse pressure gradient boundary condition development

In order to generate the desired self-similar APG TBL flow the farfield wall normal velocity BC must be modified. From Mellor & Gibson (1966)[3] the freestream streamwise velocity $u_{APG}(x) \propto x^m$ where $m = -0.23$ for the incipient separation APG TBL ($u_\tau \to 0$). The wall normal suction velocity $v_{APG}(x)$ is deduced from $u_{APG}(x)$ via the boundary layer streamfunction solution in the farfield region to be

$$v_{APG}(x) = -\frac{\partial u_{APG}(x)}{\partial x}\left[y_{BC} - \delta^*(x)\right] + u_{APG}(x)\frac{\partial \delta^*(x)}{\partial x}\ , \qquad (2)$$

where y_{BC} is the wall normal position of the farfield boundary[3]. Note for the case of a constant streamwise velocity (zero streamwise derivative), as in the ZPG TBL, (2) becomes equivalent to (1).

The structure of the complete farfield wall normal BC, $v_\infty(x)$, is as follows. In the APG TBL DNS, to allow the rescaling necessary for the inlet BC an initial ZPG TBL is simulated up until the streamwise position $x_s = 100\delta_{99,I}$ (located after the recycling plane) by applying $v_{ZPG}(x)$ as defined in (1). Downstream of the position $x_f = 140\delta_{99,I}$ the wall normal velocity $v_{APG}(x)$ is applied at the farfield boundary as given by (2), which imparts the desired deceleration and hence expansion of the boundary layer. From x_s to x_f the velocity $v_{APG}(x)$ is gradually introduced using a smoothing function. Finally the farfield velocity is transitioned from suction ($v_\infty(x) > 0$) at $x_o = 760\delta_{99,I}$ to blowing ($v_\infty(x) < 0$) at the outlet to reduce the number of instantaneous reversed flow events, such that numerical stability of the outflow boundary condition is maintained. The structure of the ZPG and APG farfield boundary conditions is illustrated in Fig. 1.

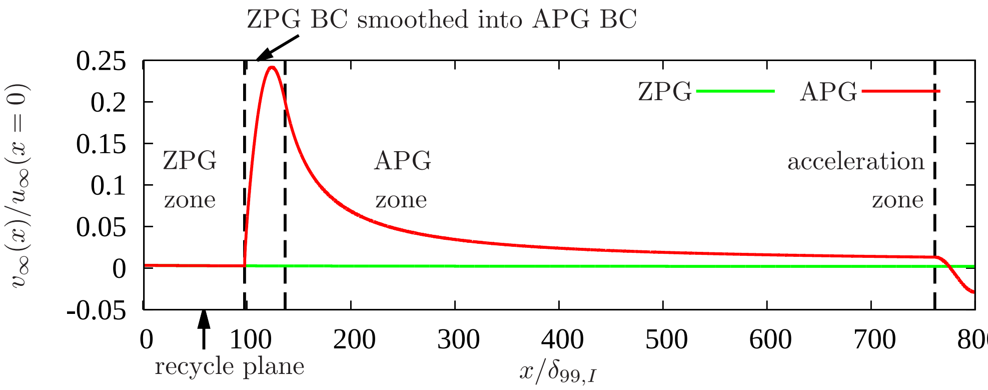

Fig. 1. Farfield wall normal velocity boundary condition in the adverse pressure gradient (red line) and zero pressure gradient (green line) direct numerical simulation.

This farfield BC was first implemented and tested in two-dimensional Reynolds Averaged Navier Stokes (RANS) simulations, yielding the appropriate self-similar velocity profiles. The BC was subsequently implemented into the DNS solver, the results of which are presented in the following section.

4. Scaling of the first and second order statistical moments

The ZPG and APG boundary layers are first compared on the basis of Re_Θ, and the friction and pressure velocity scales. The mean velocity deficit and Reynolds stress profiles from various streamwise locations are then presented in both friction and pressure velocity scaling. In all of the following figures the green and red lines represent the ZPG and APG cases respectively.

The momentum thickness based Reynolds number illustrated in Fig. 2(a), increases in the APG TBL more rapidly than the ZPG TBL, as the former expands more rapidly (hence larger Θ) in the streamwise direction as it decelerates. This deceleration of the flow also reduces the friction velocity $u_\tau = \sqrt{\tau_w/\rho}$, where τ_w is the mean shear stress at the wall. In Fig. 2(b), u_τ of the APG case is less than that of ZPG TBL as the former is decelerated more than the latter. However, the APG TBL DNS has not yet attained the desired $u_\tau \to 0$ condition, representative of the incipient separation case. Further fine tuning of the BC is required. To achieve a self-similar boundary layer the ratio of the pressure velocity (u_P) to u_∞ must be constant. The pressure velocity, defined by $u_P = \sqrt{(\partial p/\partial x)\delta^*/\rho}$, is a velocity scale based on the streamwise pressure gradient $\partial p/\partial x$. As illustrated in Fig. 2(c) a near constant ratio of u_P/u_∞ is achieved over a streamwise domain from $180\delta_{99,I}$ to $650\delta_{99,I}$.

Mean streamwise velocity deficit profiles ($u_\infty - \overline{u}$) are now presented at the streamwise locations indicated by the arrows in Fig. 2(c). In Fig. 3(a) the deficit profiles are non-dimensionalised by u_τ and plotted against y/δ_{99}, where δ_{99} is the boundary layer thickness. The blue dots in this figure represent results from the previous ZPG DNS of Jiménez et al. (2010) [13], which agree with the present ZPG simulation. When scaled by u_τ, the non-dimensional velocity profiles do not collapse, but in fact increase in the downstream direction - indicated by the arrow - as u_τ decreases. However, the profiles do collapse when scaled by u_P as illustrated Fig. 3(b). Note the ZPG profiles are not included in this figure as $u_P = 0$ in this case.

As undertaken for the velocity deficit profiles, the second order statistical moments are now presented scaled on the basis of both the wall shear stress and pressure gradient. Under the former scaling the Reynolds stress profiles are nondimensionalised using a velocity scale of u_τ and length scale of ν/u_τ. Under the latter scaling the pertinent velocity and length scales are u_P and δ^*. Profiles of the variance of the fluctuating component of the streamwise velocity ($\overline{u'u'}$) are plotted in friction velocity scaling in Fig. 3(c), which also increase as u_τ decreases in the downstream direction. Additionally a second outer peak is evident, which becomes more

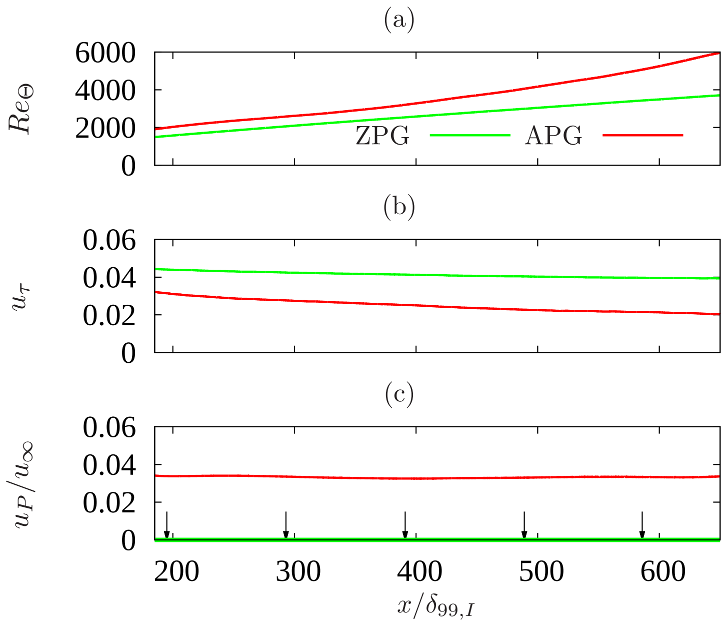

Fig. 2. Boundary layer properties of the adverse pressure gradient DNS (red line) and the zero pressure gradient DNS (green line): (a) momentum thickness Reynolds number $Re_\Theta = u_\infty \Theta/\nu$; (b) friction velocity $u_\tau = \sqrt{\tau_w/\rho}$; (c) pressure velocity $u_P = \sqrt{(\partial p/\partial x)\delta^*/\rho}$ divided by the freestream velocity u_∞, with arrows indicating the positions of the APG TBL velocity profiles illustrated in Fig. 3 and Fig. 4.

evident in the downstream direction. Similar observations are also made concerning the wall normal velocity variance, $\overline{v'v'}$, spanwise velocity variance, $\overline{w'w'}$, and Reynolds stress, $\overline{u'v'}$, plotted under friction velocity scaling in Fig. 4(a), Fig. 4(c), and Fig. 4(e) respectively. All of these Reynolds stresses increase in magnitude as u_τ decreases in the downstream direction, with a prominent second outer peak becoming stronger downstream. This outer peak collapses for all of the streamwise stations when plotted in pressure velocity scaling as illustrated for $\overline{u'u'}$, $\overline{v'v'}$, $\overline{w'w'}$ and $\overline{u'v'}$ in Fig. 3(d), Fig. 4(b), Fig. 4(d), and Fig. 4(f) respectively.

5. Concluding remarks

Development of a farfield boundary condition for the direct numerical simulation of an adverse pressure gradient turbulent boundary layer at the verge of separation has been presented. A region of constant ratio of pressure velocity to freestream velocity is attained over a momentum thickness based Reynolds number range of $Re_\theta \approx 2000$ to 6000. Mean velocity deficit profiles were shown to collapse under pressure velocity scaling, but not in friction velocity scaling. The Reynolds stresses also exhibit a second outer peak, which collapses under pressure velocity scaling.

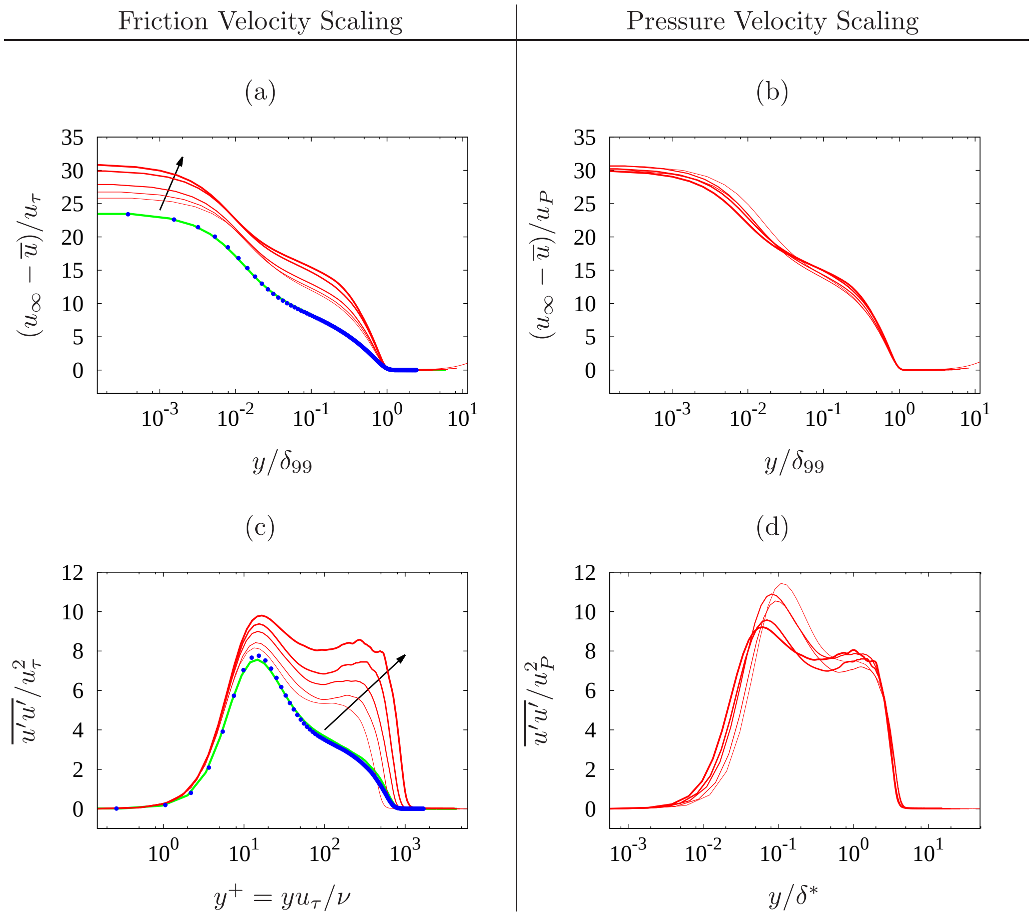

Fig. 3. Mean velocity deficit profiles nondimensionalised by: (a) friction velocity (u_τ) and boundary layer thickness (δ_{99}); and (b) pressure velocity (u_P) and displacement thickness (δ^*). Reynolds stress profile $\overline{u'u'}$ nondimensionalised by: (c) u_τ and viscous length scale ν/u_τ; and (d) u_P and δ^*. ZPG TBL DNS of Jiménez et al. (2010)[13] - blue dots; ZPG TBL DNS current simulation - green line; APG TBL DNS from current simulation at different streamwise locations - red lines, of thickness increasing with downstream position. Arrows in the left column indicate the direction of increasing x position. Positions of the APG TBL profiles are illustrated in Fig. 2(c).

Acknowledgements

The authors would like to acknowledge the research funding from the Australian Research Council and European Research Council, and the computational resources provided by the Australian National Computational Infrastructure, iVEC and PRACE. Julio Soria gratefully acknowledges the support of an Australian Research Council Discovery Outstanding Researcher Award fellowship.

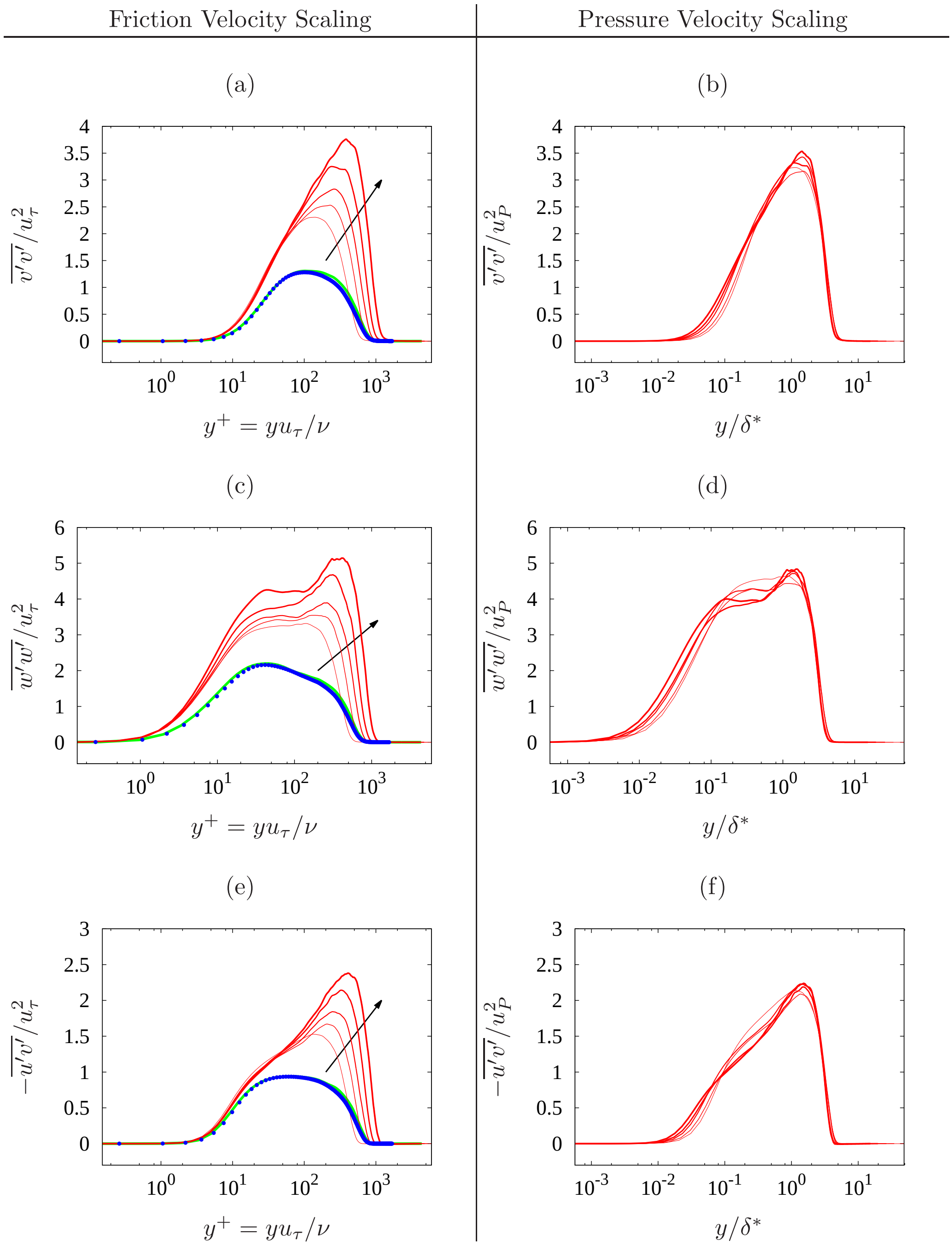

Fig. 4. Reynolds stress profiles: (a) $\overline{v'v'}$ nondimensionalised by friction velocity (u_τ) and viscous length scale ν/u_τ; (b) $\overline{v'v'}$ nondimensionalised by pressure velocity (u_P) and displacement thickness (δ^*); (c) $\overline{w'w'}$ nondimensionalised by u_τ and ν/u_τ; (d) $\overline{w'w'}$ nondimensionalised by u_P and δ^*; (e) $\overline{u'v'}$ nondimensionalised by u_τ and ν/u_τ; and (f) $\overline{u'v'}$ nondimensionalised by u_P and δ^*. ZPG TBL DNS of Jiménez et al. (2010)[13] - blue dots; ZPG TBL DNS current simulation - green line; APG TBL DNS from current simulation at different stream wise locations - red lines, of thickness increasing with downstream position. Arrows in left column indicate the direction of increasing x position. Positions of the APG TBL profiles are illustrated in Fig. 2(c).

References

1. V. Kitsios, L. Cordier, J.-P. Bonnet, A. Ooi and J. Soria, On the coherent structures and stability properties of a leading edge separated airfoil with turbulent recirculation, *J. Fluid Mech.* **683**, 395 (2011).
2. P. Skåre and P.-A. Krogstad, A turbulent equilibrium boundary layer near separation, *J. Fluid. Mech.* **272**, 319 (1994).
3. G. Mellor and D. Gibson, Equilibrium turbulent boundary layers, *J. Fluid. Mech.* **24**, 225 (1966).
4. A. Gungor, M. Simens and J. Jiménez, Direct numerical simulation of wake-perturbed separated boundary layers, *J. Turb* **134**, p. 061024 (2012).
5. J.-H. Lee and J. Sung, Effects of an adverse pressure gradient on a turbulent boundary layer, *Int. J. Heat Fluid Fl.* **29**, 568 (2008).
6. M. P. Simens, J. Jiménez, S. Hoyas and Y. Mizuno, A high-resolution code for tubulent boundary layers, *J. Comp. Phys.* **228**, 4128 (2009).
7. G. Borrell, J. Sillero and J. Jiménez, A code for direct numerical simulation of turbulent boundary layers at high reynolds numbers in BG/P supercomputers, *Comp. Fluids* **80**, 37 (2013).
8. F. Harrow and J. Welch, Numerical calculation of time-dependent viscous incompressible flow of fluid with free surface, *Phys. Fluids* **8** (1965).
9. J. Perot, An analysis of the fractional step method, *J. Comput. Phys.* **108**, 51 (1993).
10. S. Lele, Compact finite difference schemes with spectral-like resolution, *J. Comput. Phys.* **103**, 16 (1992).
11. J. Sillero, J. Jiménez and R. Moser, One-point statistics for turbulent wall-bounded at reynolds numbers up to $\delta^+ \approx 2000$, *Phys. Fluids* **25**, p. 105102 (2013).
12. J. Sillero, High Reynolds number turbulent boundary layers, PhD thesis, Universidad Politénica de Madrid, (2014).
13. J. Jiménez, S. Hoyas, M. Simens and Y. Mizuno, Turbulent boundary layers and channels at moderate Reynolds numbers, *J. Fluid. Mech.* **657**, 335 (2010).